



Size-selective mesoporous silica-based Pt(II) complex as efficient and reusable photocatalytic material



Daniel González-Muñoz^a, Antonio Casado-Sánchez^a, Isabel del Hierro^b, Santiago Gómez-Ruiz^{b,*}, Silvia Cabrera^{c,d,*}, José Alemán^{a,d,*}

^aOrganic Chemistry Department, Science Faculty, Universidad Autónoma de Madrid, 28049 Madrid, Spain

^bDepartamento de Biología y Geología, Física y Química Inorgánica, Escuela Superior de Ciencias Experimentales y Tecnología, Universidad Rey Juan Carlos, 28933 Móstoles, Madrid, Spain

^cInorganic Chemistry Department, Science Faculty, Universidad Autónoma de Madrid, 28049 Madrid, Spain

^dInstitute for Advanced Research in Chemical Sciences (IAChem), Universidad Autónoma de Madrid, 28049 Madrid, Spain

ARTICLE INFO

Article history:

Received 17 January 2019

Revised 2 April 2019

Accepted 10 April 2019

Keywords:

Mesoporous silica

Photocatalyst

Debromination

Size selectivity

Platinum(II) complex

ABSTRACT

The grafting of a Pt(II) photocatalyst into three different mesoporous silica-based materials with different particle sizes and pore sizes was easily achieved through an amide bond formation. The analysis and results of the different characterization techniques showed that the catalyst is immobilized inside the pores of the materials and the photophysical properties of the catalyst are preserved after the covalent anchoring. The photocatalytic material catalyzed efficiently the debromination reaction of different substrates and is reused without detriment in its catalytic activity. In addition, the incorporation of the catalyst into mesoporous silica materials with different pore size allows the selective debromination of substrates by size discrimination.

© 2019 Elsevier Inc. All rights reserved.

1. Introduction

The development of sustainable and greener methodologies has become an important and interesting topic in the scientific community. In this area, the use of the solar energy as energy source, by means of photocatalysis, has paved the way for water splitting, CO₂ conversion and the development of novel organic transformation among other applications [1]. Regarding the organic chemistry field, photocatalysis has been established as a powerful tool for the selective activation of different bonds using mild conditions and visible light as the driving force [2]. Despite of its growing development in the last years, most of the attention has been focused on the use of homogeneous photocatalysts, in which organic dyes and Ru(II) or Ir(III) metal complexes are the most used. By contrast, the development of heterogeneous photocatalysts for organic transformations [3] have been much less explored despite of the advantages of the heterogeneous catalysis and the successful application of heterogeneous photocatalytic systems based on semiconductor materials in other fields, such as the degradation

of pollutants in water, water splitting, CO₂ conversion to hydrocarbons or methanol photoreforming to obtain hydrogen [4].

In the field of heterogeneous catalysis, mesoporous silica-based materials have shown great potential due to the excellent physicochemical properties, high stability and inertness, high surface area, large and tunable pore sizes and shapes, and easy functionalization of the outer and inner surfaces [5]. These features allow the easy modulation of the morphology and local environment of the confined catalytic site. In addition, the silica matrix is inert to light which, together with the previously commented properties, made mesoporous silicas excellent materials for the grafting of photocatalysts and the exploration of their application in heterogeneous photocatalysis. In this context, three mesoporous silica materials with the incorporation of metallic photocatalysts have been described (top, Fig. 1) [3a–d]. Wu and Yamashita independently reported the incorporation of platinum complexes for photosensitized oxidations [3a,b]. Later, Yamashita described the synthesis and characterization of phosphorescence Ir(III) complex anchored to mesoporous silica [3c]. In 2015, Zhao showed the synthesis of a reusable heterogeneous photocatalyst based on ruthenium complex and its application for the synthesis of 2-arylpyridines under visible light conditions [3d]. Although these are beautiful examples in the immobilization of metallic complexes, these works did not study the substrate size

* Corresponding authors.

E-mail addresses: santiago.gomez@urjc.es (S. Gómez-Ruiz), silvia.cabrera@uam.es (S. Cabrera), jose.aleman@uam.es (J. Alemán).

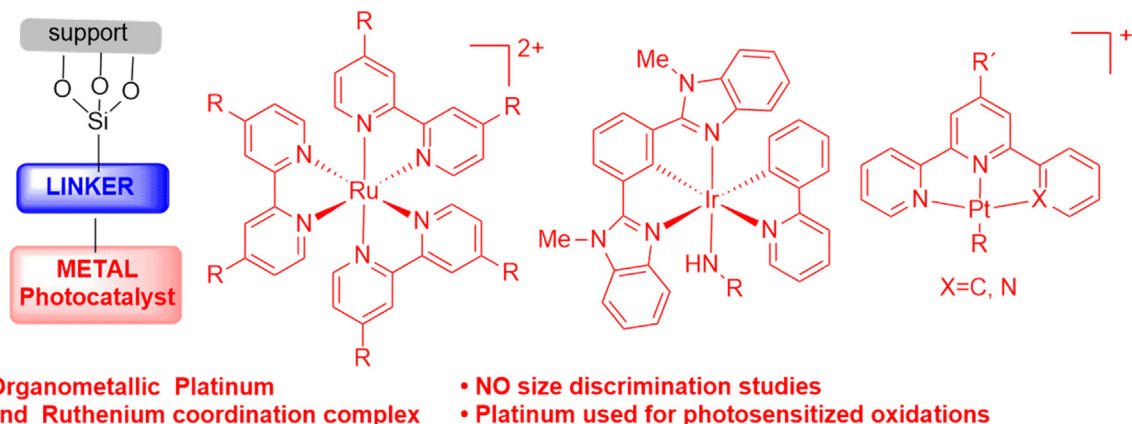
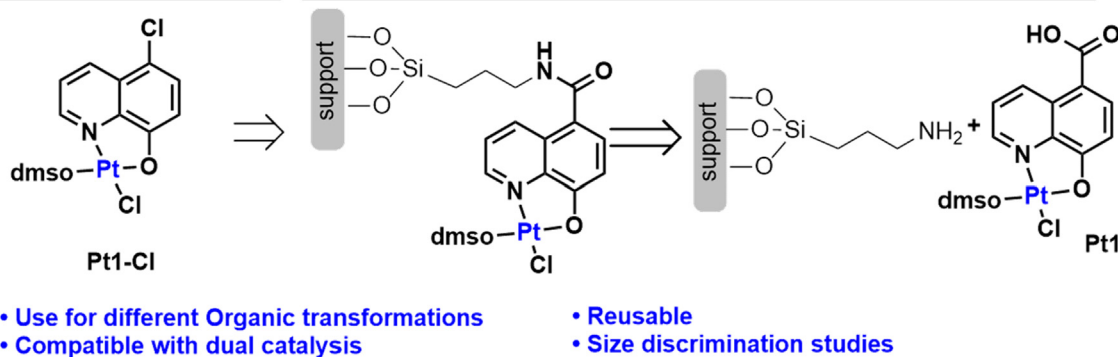
Past works:*Porous Silica Based Heterogeneous Photocatalyst***Present work:***Homogeneous photocatalyst Heterogeneous photocatalyst*

Fig. 1. Design of the heterogeneous Pt(II) photocatalyst.

selectivity by the different pores and size of mesoporous materials in relation with their photocatalytic activity.

In our research group, we developed a novel family of Pt(II) photocatalysts based on 8-hydroxyquinolines (bottom-left, Fig. 1) [6]. The most active photocatalyst (**Pt1-Cl**), that contained a 5-chloro-8-hydroxyquinoline as ligand, was able to oxidize a large number of sulfides with complete chemoselectivity in good yields using both, batch and flow processes (Fig. 1). The main drawback of the photocatalyst is the high prize of platinum compared to other more abundant metals. Therefore, we envisioned that the immobilization of the platinum complex onto mesoporous silicas might afford a recyclable catalyst, which would reduce, not only the price of the catalyst, but also time-processing, waste and costs in large-scale photocatalytic processes. In addition, with a rational tuning of the structural feature of the solid support, the heterogeneous system may also be able to discriminate reagents due to the pore structure, modulating the selectivity of the catalytic process. Therefore, in order to anchor the platinum complex, the chlorine substituent in the aromatic ring of the ligand has been changed into a carboxylic acid that will allow us to anchor to the mesoporous silica through an amide bond (Fig. 1). Herein, we report the synthetic approach for the preparation of the heterogeneous photocatalyst that involves the attachment of the catalyst **Pt1** by post-functionalization of the silica material through an amino-propyl linker. This synthetic strategy has been used for the immobilization of Pt(II) photocatalyst **Pt1** onto 3 different mesoporous silica materials (MSN, SBA-15, MSU-2) with different properties

and, their syntheses and a full characterization study by a set of different techniques is described. Finally, this work also presents a detailed study of the catalytic activity of the synthesized systems on the debromination of different organic bromide substrates, including pore-size selectivity, reusability, and its application in a dual catalytic system for the alkylation of aldehydes.

2. Experimental section

The synthesis of MSN, MSU-2 and SBA-15 materials [7], and their functionalization with 3-aminopropyltriethoxysilane [8] were carried out following literature procedures. In this section, a selection of different procedures is described. See S.I. for the full experimental section, including general methods and materials, experimental procedures, full characterization graphs and instrumental details.

2.1. Synthesis of photocatalyst **Pt1 [6,9]**

A solution of 8-hydroxy-5-quinolinecarboxylic acid (**L1**) [10] (0.30 mmol) in 0.6 mL of acetone was added to a solution of NaOH in 0.3 mL of MeOH. Then, *cis*-PtCl₂(dmso)₂ [11] (0.25 mmol) was added and the reaction mixture was stirred for 24 h at room temperature. The resulting brown solid was filtered, washed with diethyl ether (2 × 10 mL) and hexane (2 × 10 mL), and dried under vacuum (78% yield).

^1H NMR (300 MHz, DMSO d_6) δ 10.02 (d, $J = 9.0$ Hz, 1H), 9.42 (d, $J = 5.1$ Hz, 1H), 8.24 (d, $J = 8.4$ Hz, 1H), 7.78 (dd, $J = 8.7, 5.1$ Hz, 1H), 6.98 (d, $J = 8.4$ Hz, 1H), 3.65 (s, 6H). ^{13}C NMR (75 MHz, MeOD- d_4) δ 151.9, 145.0, 142.3, 141.7, 130.6, 130.3, 128.7, 122.4, 121.1, 46.5. ^{195}Pt NMR (64 MHz, MeOD- d_4) δ -2768.9 (s).

2.2. Synthesis of heterogeneous catalyst MSN-AP-Pt1, MSU-2-AP-Pt1 and SBA-15-AP-Pt1

First, a buffer of NaCl (2.92 g, 50 mmol) and morpholinoethane sulfonic acid monohydrate (MES, 2.13 g, 10 mmol) in 100 mL of Milli-Q water was prepared. Then, 40 mg of **Pt1** was dissolved in 10 mL of DMSO and subsequently added to the buffer. Next, *N*-(3-dimethylaminopropyl)-*N'*-ethylcarbodiimide hydrochloride (EDC, 40 mg, 0.26 mmol), *N*-hydroxysuccinimide (NHS, 60 mg, 0.52 mmol), 2-mercaptoethanol (0.17 mL, 2.42 mmol) and the corresponding aminopropyl-functionalized material (400 mg) were added. The reaction mixture was stirred for 2 h at rt and then hydroxylamine hydrochloride (83 mg, 2.52 mmol) was added. A yellow solid was formed which was isolated by centrifugation and washed with Milli-Q water (3×30 mL) and diethyl ether (3×30 mL).

2.3. Photocatalytic debromination of organic bromides

An oven-dried 10 mL glass vial was loaded with the corresponding heterogeneous Pt complex (1 mol% of Pt). Then, 1 mL of absolute ethanol, *N,N*-diisopropylethylamine (0.3 mmol) and the corresponding organic bromide **1** (0.1 mmol) were added to the vial. The reaction mixture was degassed by three cycles of freeze-pump-thaw. Next, the reaction was stirred under irradiation using a custom-made “light box” (see S.I.) at rt. After 24 h, the reaction mixture was filtered over Celite® and the crude was purified by flash chromatography to afford the corresponding debrominated product **2**.

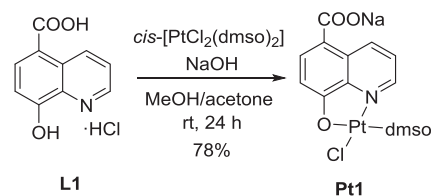
2.4. Photocatalytic α -alkylation of aldehydes

To an oven-dried 10 mL glass vial were added MSN-AP-Pt1 (1 mol% of Pt), diethyl 2-bromomalonate **1a** (0.1 mmol), the corresponding aldehyde **3** (0.2 mmol) and MacMillan's imidazolidinone catalyst (20 mol%). Then, 200 μL of anhydrous DMF and 2,6-lutidine (0.2 mmol) were added to the vial. The vial was sealed with a PTFE/rubber septum and the reaction mixture was degassed by three cycles of freeze-pump-thaw. Afterwards, the reaction mixture was stirred and irradiated using blue LED irradiation (see S.I. for more details) at rt. The reaction progress was monitored by ^1H NMR.

3. Results and discussion

3.1. Synthesis and characterization of the heterogeneous catalyst

The platinum photocatalyst **Pt1** was prepared according to a procedure previously reported by us [6,9], by the complexation of the 8-hydroxyquinoline derivative ligand (**L1**) [10] and the platinum precursor $[\text{PtCl}_2(\text{dmsO})_2]$ [11] using NaOH as base in a mixture of methanol/acetone at room temperature. Following these conditions, the sodium carboxylate complex **Pt1** was isolated in 78% yield (Scheme 1). The ^1H and ^{13}C NMR chemical shifts of the complex **Pt1** showed a downfield shift of most of the ^1H or ^{13}C signals compared to those of the free **L1**, which confirmed the complexation of the ligand **L1** to the metal. In addition, complex **Pt1** was also characterized by ^{195}Pt NMR, observing a signal at ca.



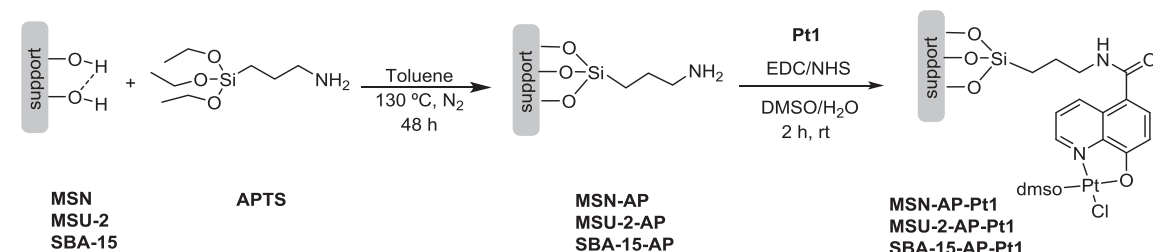
Scheme 1. Synthesis of complex **Pt1**.

–2768 ppm which is in agreement with chemical shifts reported for similar platinum(II) complexes [6,9].

In order to explore the catalytic performance of the catalyst **Pt1** in a heterogeneous system, MSN, MSU-2 and SBA-15 materials have been chosen as supports for the immobilization of the platinum complex [7]. These three silica-based mesoporous materials present the same chemical composition but different particle size, pore size and morphology, and different arrangements of the porous structure. Whereas MSN are silica spheres with hexagonal arrangement of the pores, SBA-15 has hexagonal arrangement of the pores too, but a bigger pore size than that of MSN. In addition, the SBA-15 particle shape is different to that of MSN as SBA-15 consists of elongated spheres of up to 700 nm and MSN in spheres of ca. 80 nm diameter. Moreover, the silica material MSU-2, with spherical morphology and wormhole-like arrangement of the pores, was also selected as support for this catalytic study. The structural differences of the different silica-based supports will allow us to study the influence of the textural and morphological properties of the silica materials into the catalytic performance of the photocatalyst. The syntheses of the silica-based materials were carried out following reported procedures [7] and were characterized by IR, X-ray powder diffraction (XRD), solid physisorption (BET), SEM and TEM, obtaining data which are in agreement with those previously described in the literature for MSN, SBA-15 or MSU-2, respectively (see S.I. for all the data). Subsequently, the mesoporous materials were functionalized with (3-aminopropyl)triethoxysilane (APTS) in order to incorporate aminopropyl (AP) groups, which will serve as linkers for the subsequent anchoring of the complex **Pt1** to the materials. The functionalization with APTS was successfully achieved for MSN, SBA-15 and MSU-2 by heating APTS and the corresponding material in toluene at high temperature (Scheme 2) [8]. The incorporation of the AP group to the materials was confirmed by IR analysis, as the characteristic stretching vibration band around 3000 cm^{-1} attributed to the presence of N-H and C-H was observed in the IR spectra of each functionalized material (see S.I.).

In the last synthetic step, the covalent anchoring of the photocatalyst **Pt1** was carried out by using a well-established coupling methodology [12] between the amino group of the AP linker of each silica-based material and the carboxylic acid of the **Pt1** catalyst (Scheme 2).

The characterization of these new synthesized materials with the platinum complex **Pt1** was conducted using different techniques: IR analysis, X-ray fluorescence (XRF), BET, XRD, SEM and TEM (see S.I.). The IR spectra of the three Pt-functionalized materials showed the specific bands of the mesoporous framework together with the corresponding bands of the aminopropyl linker. In addition, the appearance of a new characteristic band corresponding to an amide C=O stretching vibration at $\sim 1650\text{ cm}^{-1}$ corroborates the tethering of the Pt(II) complex onto the material. Moreover, the IR band corresponding to the unmodified carboxylic acid was not detected, indicating that all the Pt catalyst is bound to the silica-based material. The BET isotherms of the three Pt-functionalized materials exhibited the typical type IV isotherm with hysteresis loops of mesoporous solids (Fig. 2). Nevertheless, the covalent anchoring of the catalyst led to lower surface areas,



Scheme 2. Synthetic pathway for the anchoring of photocatalyst **Pt1** into the silica.

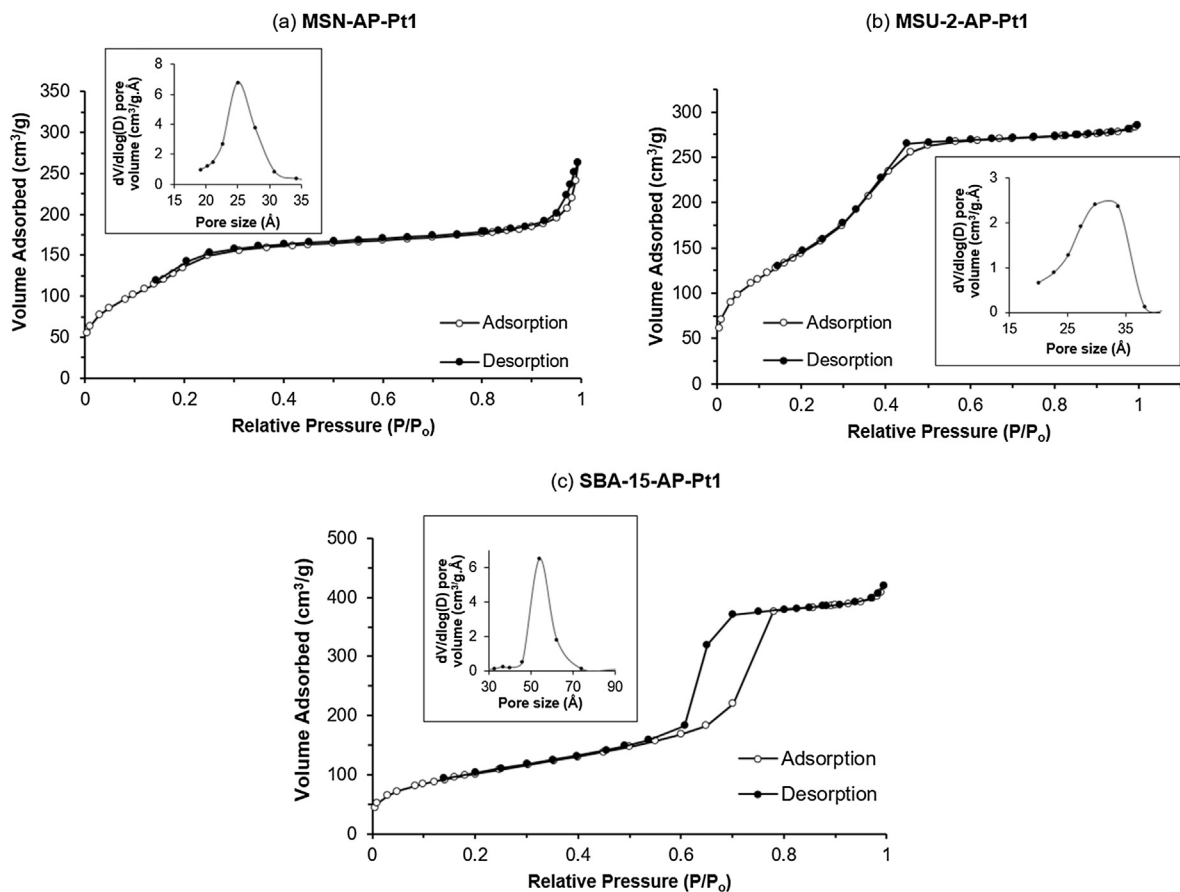


Fig. 2. N_2 adsorption-desorption isotherms and pore size distribution (insert) of **MSN-AP-Pt1** (a), **MSU-2-AP-Pt1** (b) and **SBA-15-AP-Pt1** (c).

pore volume and pore size compared to those of the unmodified MSN, SBA-15 and MSU-2 in each case (Fig. 2 and Table 1). Therefore, the functionalization of the MSN material to **MSN-AP-Pt1** involves a decrease in the pore size from 2.5 to 2.1 nm. Similarly, a pore size decrease was also observed for the functionalized materials **MSU-2-AP-Pt1** and **SBA-15-AP-Pt1** on direct comparison with their corresponding unmodified analogues MSU-2 and SBA-15. The

decrease in the pore size of the three Pt-functionalized materials indicates that the anchoring of the catalyst has mainly taken place within the pores and channels of the material. In addition, the platinum content of the materials was determined by XRF analysis, observing that **MSN-AP-Pt1** has a 4.5% Pt content, while **MSU-2-AP-Pt1** and **SBA-15-AP-Pt1** have a 6.6% and 2.3%, respectively. To determine the degree of functionalization of the materials, the

Table 1

Summary of the main physico-chemical parameters of the heterogeneous catalysts and the parent materials.

Material	a_0 (Å)	Pore size (Å)	Surface area (m^2/g)	Pore volume (cm^3/g)	Pt content (% w/w)
MSN	42.15	25.0	1017	1.57	–
MSU-2	60.09	33.6	961	0.95	–
SBA-15	111.14	65.2	781	0.96	–
MSN-AP-Pt1	43.83	21.0	513	0.39	4.5
MSU-2-AP-Pt1	58.14	30.0	535	0.49	6.6
SBA-15-AP-Pt1	100.24	54.0	372	0.66	2.3

ratio Pt/N has been calculated from the elemental analysis. The calculated ratio Pt/N of the three materials is in agreement with their Pt content determined by XRF. Therefore, **MSU-2-AP-Pt1** material contains the highest Pt/N ratio (1/3), whereas lower degrees of functionalization were achieved for the two materials with hexagonal pore distribution, **MSN-AP-Pt1** and **SBA-15-AP-Pt1** (1/6.7 and 1/10.6, respectively). These results shown that the most effective functionalization rate was found for MSU-2 material, as it was previously reported by us [7c].

Finally, the morphology and structure of the platinum supported materials was analyzed by powder XRD, SEM and TEM. The XRD patterns of the functionalized materials indicate that the ordered mesoporous structure is retained after the anchoring of the catalyst (see S.I) as the obtained diffractograms showed similar diffraction patterns than those of the unmodified silica materials MSN, SBA-15 and MSU-2 with the unique difference of a reduction in the intensity of the peaks. The decrease in the intensity of the diffraction peaks is due to the incorporation of the Pt-catalyst into the pore, which is usually associated with a partial blocking of the dispersion points of the pores. Moreover, the SEM and TEM images of the supported materials (Fig. 3 and S.I) demonstrate that the morphology and pore arrangement of the platinum supported-materials is retained after functionalization observing that, in all cases, the morphology and particle size is not modified in the functionalization processes.

In addition, the elemental mapping of C, Pt, and Si of the supported material **MSN-AP-Pt1** was measured by SEM. As shown in Fig. 4, the material presents a uniform distribution of C, Si and, more important, of Pt, which clearly supports the highly dispersed incorporation of the Pt-catalyst throughout the material.

3.2. Photophysical properties

To further determine the potential suitability of the Pt-functionalized materials as photocatalysts, their photophysical and electrochemical properties were studied. Firstly, the diffuse reflectance spectra of the three Pt-functionalized materials was recorded (Fig. 5a). The spectrum of the three Pt-functionalized materials show a band centered at ~ 420 nm, which corresponds to the MLCT band of the complex **Pt1**. A comparison between the maximum absorption wavelengths of the homogeneous Pt compound (see Fig. 5b) and the heterogeneous Pt-functionalized materials shows that the absorption properties of the materials are due to the Pt complex, and the silica materials do not modify the main photophysical properties of the photocatalyst. It is important to note that the difference in intensity of the bands could be attributed to the different Pt content of the materials (see Table 1). Furthermore, we have also verified that neither the silica supports nor the aminopropyl-modified materials present any significant band in their diffuse reflectance spectra, confirming that both the

silica and the aminopropyl moiety do not interact with the irradiation light.

The photoluminescence of the three Pt-functionalized materials was studied at room temperature and 77 K using degassed EtOH solutions of highly dispersed samples (Fig. 5c–d). The emission spectra at rt of the three materials presents two maximums at ~ 485 and 529, whereas the **MSN-AP-Pt1** material contains an additional maximum at 607 nm. Moreover, the intensity of the emission depends on the Pt content of the material, being **MSU-2-AP-Pt1** the most photoluminescence material (6.6% Pt, see Table 1). On the other hand, at lower temperatures (77 K) a unique band in the range of 575–600 nm is recorded. It is importance to notice the bathochromic shift of the emission band of the supported **Pt1** complex depending on the pore size of the mesoporous silica material, which is more significant in the case of the emission at lower temperatures (Fig. 5d). This bathochromic shift in the emission spectra of molecules inside inorganic materials such as zeolites and mesoporous silica depending on the pore size has been attributed to the orbital-confinement effect of the inorganic material [13]. Briefly, the confinement effect of the inorganic material into the guest molecule (the **Pt1** complex in our case) generates an overall reduction of the HOMO-LUMO energy gap of the guest molecule and, consequently, shifts the emission band at higher wavelengths. The spectra shown in Fig. 5d are consistent with the confinement effect as the emission band of the **Pt1** catalyst shows a bathochromic shift when the pore size of the material decreases (pore size: 54 Å for **SBA-15-AP-Pt1**, 30 Å for **MSU-2-AP-Pt1**, 21 Å for **MSN-AP-Pt1**).

The ground-state redox potentials of the functionalized materials were determined by cyclic voltammetry (CV) in acetonitrile as solvent. The three Pt-containing materials present an oxidation peak close to +1.40 V (vs Ag/AgCl), which corresponds to the Pt(II)-Pt(III) oxidation. Moreover, the reduction peak was not possible to be detected. Taking into account the ground state redox potentials and the long wavelength tail of the absorption spectrum, the oxidation excited state potentials of the heterogeneous Pt(II) catalysts were estimated to be -1.38 V for **MSN-AP-Pt1**, -1.34 V for **MSU-2-AP-Pt1** and -1.35 V for **SBA-15-AP-Pt1** (V vs Ag/AgCl) (see S.I). These values indicate that the environment of the silica material does not produce a significant effect in the photophysical parameters of the Pt(II) photocatalyst in comparison with the homogenous catalyst (**Pt1-Cl**, -1.24 V vs Ag/AgCl).

3.3. Catalytic activity

The heterogeneous catalysts **MSN-AP-Pt1**, **SBA-15-AP-Pt1** and **MSU-2-AP-Pt1** were evaluated in the debromination of organic molecules as a model reaction. The reactions were carried out under nitrogen atmosphere using different bromoderivatives, diisopropylethylamine (DIPEA) as electron and/or hydrogen atom donor, in ethanol as solvent and using blue LED ($\lambda_{\max} = 450$ nm)

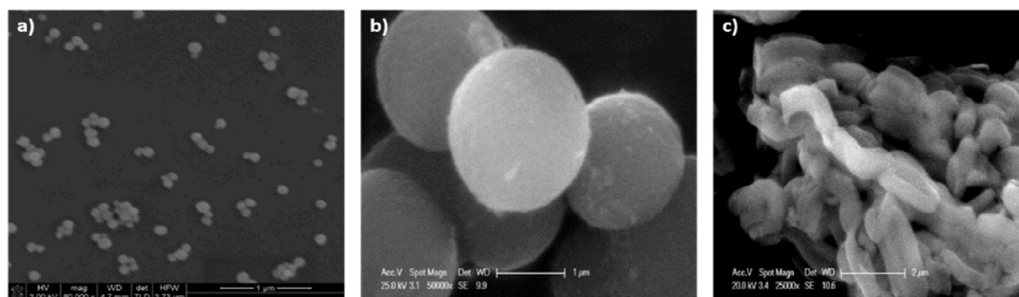


Fig. 3. SEM images of **MSN-AP-Pt1** (a), **MSU-2-AP-Pt1** (b), **SBA-15-AP-Pt1** (c).

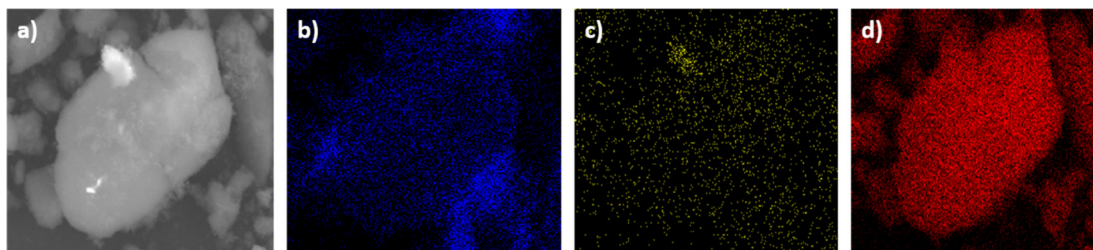


Fig. 4. SEM image (a), mapping of C (b), mapping of Pt (c) and mapping of Si (d) of supported material **MSN-AP-Pt1**.

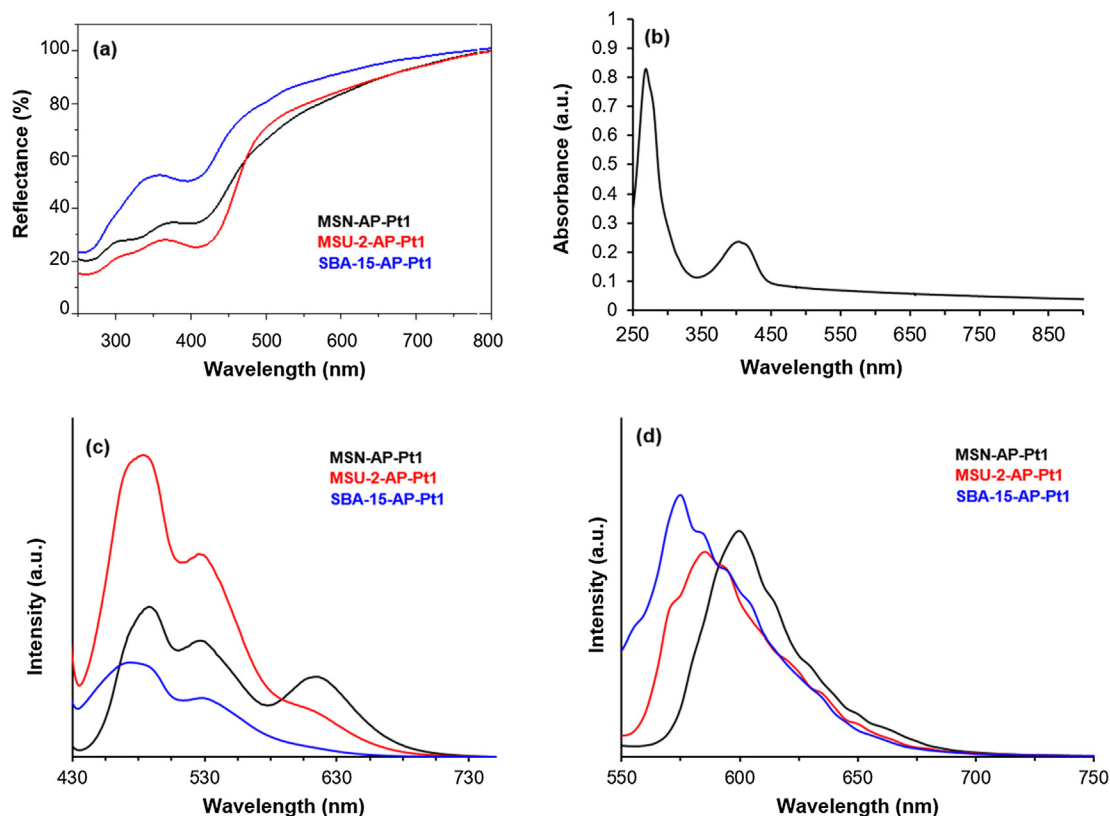
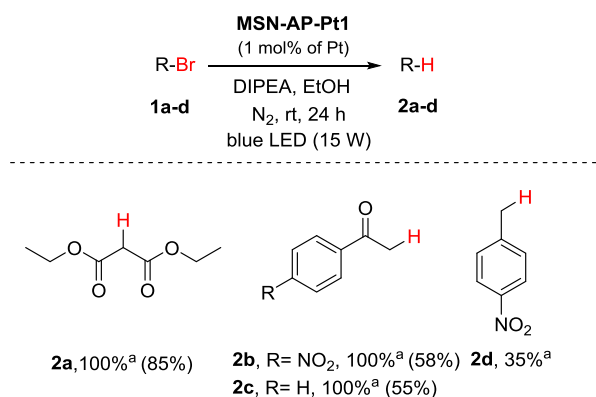


Fig. 5. (a) Solid reflectance UV-Vis spectra of the materials and (b) UV-Vis absorbance of homogeneous complex **Pt1**. (c) Luminescence spectra of the materials at rt ($\lambda_{\text{ex}} = 410$ nm). (d) Luminescence spectra of the materials at 77 K ($\lambda_{\text{ex}} = 410$ nm).



^a Conversions determined by ¹H NMR analysis of the crude mixture. Yields of isolated products between brackets.

Scheme 3. Debromination of different substrates using **MSN-AP-Pt1** as photocatalyst.

as irradiation source (Scheme 3). To evaluate the catalytic activity of the materials, the platinum(II) loaded MSN material (**MSN-AP-Pt1**) was chosen as heterogeneous catalyst. After 24 h, **MSN-AP-Pt1** is able to completely debrominate the diethyl bromomalonate (**1a**) and the 2-bromoacetone derivatives **1b** and **1c**. In contrast, the more difficult compound to debrominate (**1d**) gave only a conversion of 35%. Moreover, the debromination of **1a** did not take place in the dark or in the absence of photocatalytic material, using silica templates (MSN, MSU-2 and SBA-15) or silica templates functionalized with APTS (MSN-AP, MSU-2-AP and SBA-15-AP), (see also other control experiment in S.I., Section 2.7, Table S1). Therefore, we demonstrate that both the light and the Pt(II) photocatalyst are required for the effective transformation into the dehalogenated products. The debromination reaction of **1a** was also carried out using a modified **MSN-AP-Pt1** material with the outer surface capped with trimethylsilyl groups (**MSN(TMS)-AP-Pt1**) and a similar platinum content (4.3%) [14]. Using this material the debromination rate of **1a** was analogous to that of the uncapped catalytic MSN material (**MSN-AP-Pt1**). Therefore, this result confirms that the functionalization of the MSN with the plat-

in(II) photocatalyst **Pt1** has mainly taken place inside the pores of the silica-based system and not in the external surface area of the nanoparticles.

Based on the good catalytic performance shown by supported catalyst **MSN-AP-Pt1**, a comparative study of the three silica-based materials was carried out to investigate the influence of pore size and morphology of the materials on the debromination rate. For this purpose, diethyl bromomalonate (**1a**) and di(*tert*-butyl) bromomalonate (**1e**) were chosen as model substrates and were submitted to the photodebromination reaction using **MSN-AP-Pt1**, **MSU-2-AP-Pt1** and **SBA-15-AP-Pt1** as photocatalysts (Fig. 6). Under the same catalytic amounts of Pt(II) complex (1 mol% of Pt), all the three materials were able to debrominate around 80% of the ethyl substrate **1a**. However, regarding the more bulky substrate **1e**, higher differences in terms of reactivity were observed

between the three catalytic materials. The two materials with hexagonal pore distribution (**MSN-AP-Pt1** and **SBA-15-AP-Pt1**) showed higher catalytic activity than **MSU-2-AP-Pt1**, being **SBA-15-AP-Pt1** the most active catalyst that converted 80% of substrate **1e** in only 4 h. This material, **SBA-15-AP-Pt1**, has a larger pore size than that of **MSN-AP-Pt1** (5.4 vs 2.1 nm, see Table 1) which facilitated the easy access and diffusion of substrate **1e** and resulted in higher catalytic efficiency. Accordingly, the poor catalytic activity of **MSU-2-AP-Pt1**, 20% conversion after 4 h, could be attributed to its irregular shape, small pore size and larger particle size that may slow down the entrance and diffusion of bigger substrates such as **1e**.

With the two best catalytic materials, **MSN-AP-Pt1**, **SBA-15-AP-Pt1**, we additionally studied a competitive debromination of the two substrates **1a** and **1e** in the same reaction media (Fig. 7). Both

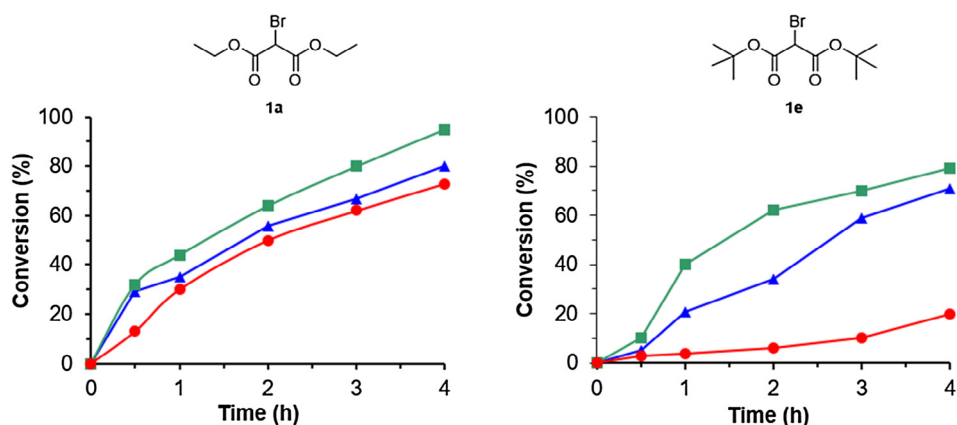


Fig. 6. Kinetic study of the debromination of substrate **1a** or **1e** using **MSN-AP-Pt1** (▲), **MSU-2-AP-Pt1** (●) and **SBA-15-AP-Pt1** (■) (1 mol% of Pt).

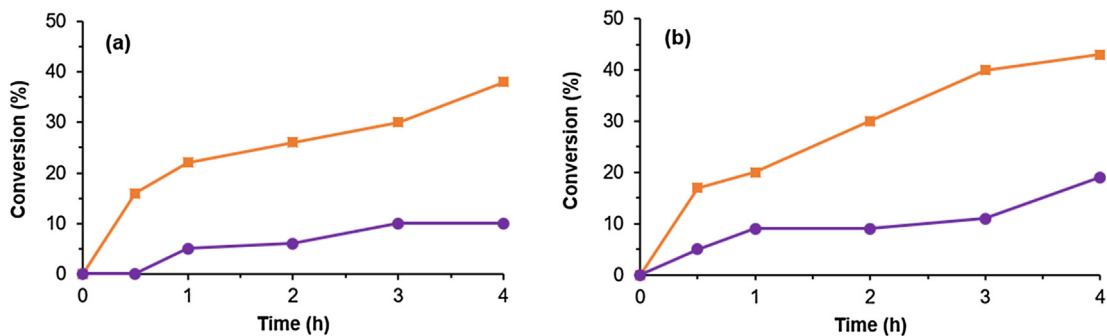


Fig. 7. Competitive study of the simultaneous debromination of the ethyl derivative **1a** (■) and *tert*-butyl derivative **1e** (●) using **MSN-AP-Pt1** (a) or **SBA-15-AP-Pt1** (b).

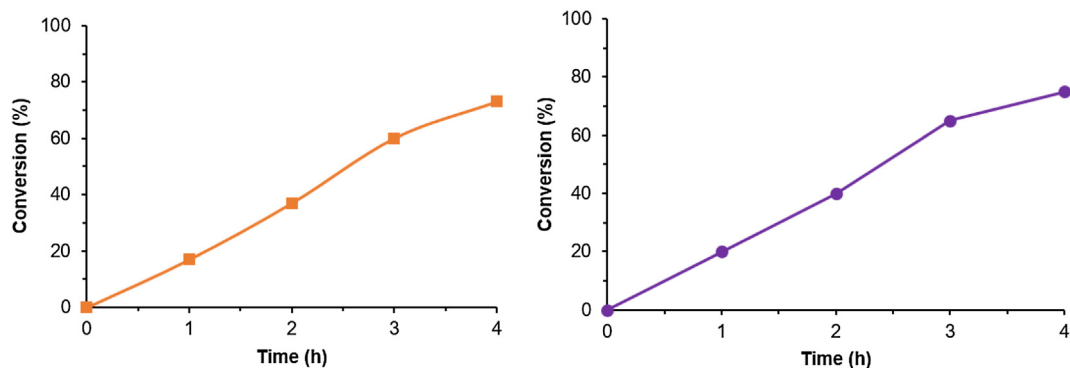


Fig. 8. Debromination of the ethyl derivative **1a** (■) and *tert*-butyl derivative **1e** (●) using **amorphous-AP-Pt1** (1 mol% of Pt).

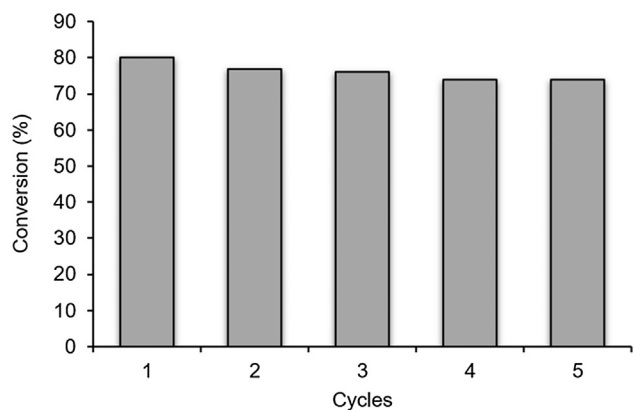
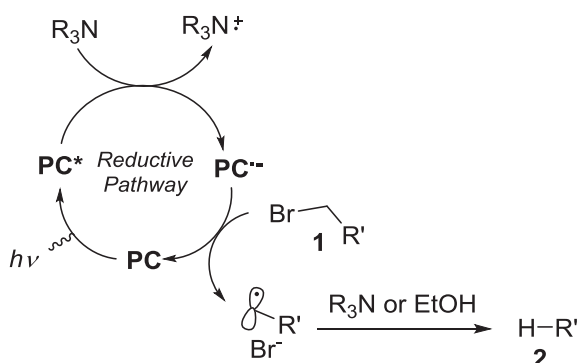


Fig. 9. Recyclability of heterogeneous catalyst **MSN-AP-Pt1** in the debromination of diethyl bromomalonate (**1a**).



Scheme 4. Postulated mechanism for the debromination of different substrates using the heterogeneous Pt(II) photocatalyst.

catalytic materials showed catalytic discrimination by the substrate size, being the conversion of the ethyl substrate **1a** much higher than that of **1e** (*tert*-butyl derivative). This discrimination is more pronounced for **MSN-AP-Pt1** catalyst, observing a

debromination rate of **1a** ca. 4-fold faster than that found for **1e**. Therefore, this is an additional indication that the functionalization of the materials with the **Pt1** complex is inside the pores of the silica-based mesoporous systems.

In order to gain more insights into the effect of the mesoporous environment in the catalytic activity of the different materials, we anchored complex **Pt1** into amorphous silica following the functionalization steps described for the other silica materials (see **Scheme 2** and SI for more details). The amount of Pt has been determined by XRF to be 2.5%. Next, the debromination of substrates **1a** and **1e** using 1 mol% of **amorphous-AP-Pt1** material was performed in different vials (**Fig. 8**). The debromination rate of both substrates is very similar, which indicates that the different photocatalytic activity of **MSN-AP-Pt1**, **SBA-15-AP-Pt1** and **MSU-2-AP-Pt1** was caused by the pores size (compared in **Figs. 6–7** and **8**).

Some of the main advantages of the heterogeneous catalysts are their easy separation from the reaction mixture, their reuse and their higher stability compared to homogeneous catalyst. In this sense and to investigate the recyclability of our heterogeneous catalyst, reusability studies of **MSN-AP-Pt1** in the debromination of diethyl bromomalonate (**1a**) were carried out. Thus, after 8 h of reaction, the mixture was centrifuged and the supernatant (reaction crude) was separated and analyzed by ^1H NMR. The catalyst was subsequently washed with ethanol, and used in a new catalytic cycle by adding fresh reactants. As shown in **Fig. 9**, the catalytic performance was maintained for at least 5 times without decrease in the catalytic activity. Furthermore, the stability of **MSN-AP-Pt1** catalyst was confirmed by recording the IR and UV–Vis spectra of the reused catalyst. Both spectra of the material remain unaltered after the reaction run (see **S.I.**). In addition, the catalyst leaching was studied treating the reaction mixture to a hot filtration [15]. After the removal of the solid catalyst at 50% of conversion, no further reaction was observed along the time. This result demonstrates that there is no homogeneous catalytically active species in solution, and the catalytic activity obtained using the heterogeneous **MSN-AP-Pt1** catalyst is only due to the anchored **Pt1** complex. In summary, these experiments show the excellent stability and reusability of the heterogeneous catalyst in the studied reactions.

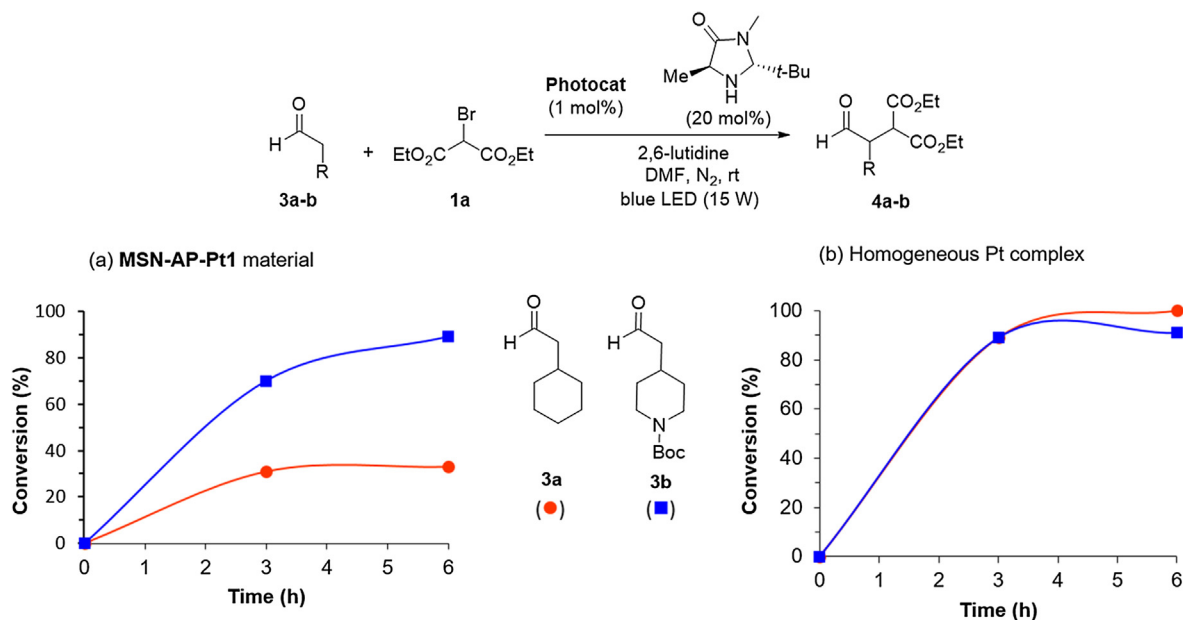


Fig. 10. (a) α -Alkylation of aldehydes **3a** and **3b** with bromoderivative **1a** using **MSN-AP-Pt1** material or (b) homogeneous **Pt1-Cl** complex as catalysts.

The mechanism proposed for the debromination of organic compounds under the heterogeneous Pt(II)-photocatalytic materials is depicted in Scheme 4. According to literature [16], the debromination of organic bromides involves a reductive quenching mechanism. Upon irradiation under visible-light, the excited state of the photocatalyst (PC^*) is reduced by diisopropylethylamine (R_3N), which acts as electron donor. Next, the reduced photocatalyst (PC^-) is oxidized by the alkyl bromoderivative (**1**) to regenerate the initial Pt(II) catalyst. Finally, the alkyl radical is protonated by diisopropylethylamine radical cation or ethanol (the solvent) to afford the final debrominated compound **2**.

With these results on hand, we decided to evaluate the potential versatility of the catalyst by extending the applicability of the photocatalytic material in some other catalytic reactions. In this context in 2008, MacMillan reported the α -alkylation of aldehydes with diethyl bromomalonate using a dual catalytic system, which combined the imidazolidinone organocatalyst and the photoredox catalyst $Ru(bpy)_3Cl_2$ [17]. Later, other complexes and organic molecules were also studied as photocatalysts for that transformation [18]. However, to the best of our knowledge, there are no reports on the use of Pt(II) complexes as photoredox catalysts for this transformation. Thus, the alkylation of aldehydes **3a** and **3b** with bromomalonate **1a** were carried out using MacMillan's organocatalyst, **MSN-AP-Pt1** as heterogeneous photocatalyst and 2,6-lutidine as base in DMF as solvent with blue LEDs as irradiation source (Fig. 10). Gratefully, the heterogeneous photocatalyst **MSN-AP-Pt1** is able to catalyze the α -alkylation of both aldehydes **3a** and **3b**, although high differences in terms of reactivity were observed [19]. During the monitoring of the reactions along the time (Fig. 10a), we observed that the alkylation rate of aldehyde **3b** was 3-fold higher than that of aldehyde **3a**. However, and taking into account that the molecular size of **3b** is higher than that of **3a**, the reactivity is completely opposite to the size selectivity of the **MSN-AP-Pt1** catalyst previously observed. After the analysis of these results, we decided to study if the different rate observed for the alkylation reaction of aldehydes **3a** and **3b** was due to the effect of the silica support or, on the other hand, to the photocatalytic activity of the Pt complex. To disclose this assumption, the alkylation of both aldehydes (**3a** and **3b**) was carried out by using the homogeneous Pt(II) photocatalyst (**Pt1-Cl**). As shown in Fig. 10b, the alkylation rate of both aldehydes with the bromoderivative **1a** using the homogeneous catalyst was very similar, indicating that the reactivity of both aldehydes and the kinetics of both transformations are comparable. Therefore, it seems that the catalytic activity of the Pt photocatalyst when supported onto the silica-based material is altered, reducing the catalytic conversion to ca. 30% in the case of **3a** [20].

4. Conclusions

The synthesis of a Pt(II) catalyst immobilized into three different mesoporous silica-based materials has been carried out. A detailed characterization study of those heterogeneous catalysts showed that the Pt(II) complex has been regularly incorporated inside the pore and the photophysical and photochemical properties of the homogeneous Pt(II) complex are preserved after immobilization. Their photocatalytic activities were evaluated in the debromination of different organic bromides, showing high debromination conversions, good recyclability and high stability (no detectable leaching). Furthermore, this investigation further confirmed that the covalent anchoring of the Pt(II) complexes into mesoporous materials allows the selective debromination of substrates by size discrimination. Moreover, our photocatalytic materials are compatible in dual catalytic processes, allowing the alkylation of aldehydes in good conversions. All these studies high-

lighted the good catalytic performance and robustness of the heterogeneous Pt(II) photocatalysts developed by our group.

Acknowledgments

This work was supported by the Ministerio de Ciencia, Innovación y Universidades from the Spanish Government (Grant no. CTQ2015-64561-R and CTQ2015-66164-R).

Appendix A. Supplementary material

Supplementary data to this article can be found online at <https://doi.org/10.1016/j.jcat.2019.04.015>.

References

- [1] (a) For selected reviews see: J. Qi, W. Zhang, R. Cao, *Adv. Energy Mater.* **8** (2018) 1701620; (b) J. Wu, Y. Huang, W. Ye, Y. Li, *Adv. Sci.* (2017) 1700194; (c) S. Zhu, D. Wang, *Adv. Energy Mater.* **7** (2017) 1700841; (d) J.K. Stolarczyk, S. Bhattacharyya, L. Polavarapu, J. Feldmann, *ACS Catal.* **8** (2018) 3602–3635.
- [2] a) C.K. Prier, D.A. Rankic, D.W.C. MacMillan, *Chem. Rev.* **113** (2013) 5322–5363; b) J.M.R. Narayanam, C.R.J. Stephenson, *Chem. Soc. Rev.* **40** (2011) 102–113; c) D. Ravelli, S. Protti, M. Fagnoni, *Chem. Rev.* **116** (2016) 9850–9913; d) C.B. Larsen, O.S. Wenger, *Chem. Eur. J.* **24** (2018) 2039–2058.
- [3] a) K. Feng, R.-Y. Zhang, L.-Z. Wu, B. Tu, M.-L. Peng, L.-P. Zhang, D. Zhao, C.-H. Tung, *J. Am. Chem. Soc.* **128** (2006) 14685–14690; b) K. Mori, K. Watanabe, M. Kawashima, M. Che, H. Yamashita, *J. Phys. Chem. C* **115** (2011) 1044–1050; c) K. Mori, M. Tottori, K. Watanabe, M. Che, H. Yamashita, *J. Phys. Chem. C* **115** (2011) 21358–21362; d) A. Jana, J. Mondal, P. Borah, S. Mondal, A. Bhaumik, Y. Zhao, *Chem. Commun.* **51** (2015) 10746–10749.
- [4] a) M. Cherevatskaya, B. König, *Russ. Chem. Rev.* **3** (2014) 183–195; b) D.P. Sahoo, D. Rath, B. Nanda, K.M. Parida, *RSC Adv.* **5** (2015) 83707–83724; c) H. Park, H. Kim, G. Moon, W. Choi, *Energy Environ. Sci.* **9** (2016) 411–433; d) B. Rico-Oller, A. Boudjemaa, H. Bahruji, M. Kebir, S. Prashar, K. Bachari, M. Fajardo, S. Gómez-Ruiz, *Sci. Total Environ.* **563–564** (2016) 921–932; e) K.C. Christoforidis, P. Fornasiero, *ChemCatChem* **9** (2017) 1523–1544.
- [5] a) F. Hoffmann, M. Cornelius, J. Morell, M. Fröba, *Angew. Chem. Int. Ed.* **45** (2006) 3216–3251; b) C. Perego, R. Millini, *Chem. Soc. Rev.* **42** (2013) 3956–3976; c) N. Pal, A. Bhaumik, *RSC Adv.* **5** (2015) 24363–24391.
- [6] A. Casado-Sánchez, R. Gómez-Ballesteros, F. Tato, F.J. Soriano, G. Pascual-Coca, S. Cabrera, J. Alemán, *Chem. Commun.* **52** (2016) 9137.
- [7] (a) For MSN see: Y. Zhao, B. Trewyn, I. Slowing, V. Lim, *J. Am. Chem. Soc.* **131** (2009) 8398–8400; (b) for SBA-15 see: D. Zhao, Q. Huo, J. Feng, B. Chmelka, G. Stucky, *J. Am. Chem. Soc.* **120** (1998) 6024–6036; (c) for MSU-2 see: D. Pérez-Quintanilla, A. Sánchez, I. Hierro, M. Fajardo, I. Sierra, *J. Nanosci. Nanotechnol.* **9** (2009) 4901–4909.
- [8] See for example: R. Kotcherlakota, A.K. Barui, S. Prashar, M. Fajardo, D. Briones, A. Rodríguez-Diéguez, C.R. Patra, S. Gómez-Ruiz, *Biomater. Sci.* **4** (2016) 448–459.
- [9] C. Martín Santos, S. Cabrera, C. Ríos-Luci, J.M. Padrón, I. López Solera, A.G. Quiroga, M.A. Medrano, C. Navarro-Ranninger, J. Alemán, *Dalton Trans.* **42** (2013) 13343–13348.
- [10] R. Schiller, G. Scozzafava, A. Tumber, J.R. Wickens, J.T. Bush, G. Rai, C. Lejeune, H. Choi, T.-L. Yeh, M.C. Chan, B.T. Mott, J.S.O. McCullagh, D.J. Maloney, C.J. Schofield, A. Kawamura, *ChemMedChem* **9** (2014) 566–571.
- [11] J.H. Price, A.N. Williamson, R.F. Schramm, B.B. Wayland, *Inorg. Chem.* **11** (1972) 1280–1284.
- [12] E. Valeur, M. Bradley, *Chem Soc. Rev.* **38** (2009) 606–631.
- [13] a) F. Márquez, H. García, E. Palomares, L. Fernández, A. Corma, *J. Am. Chem. Soc.* **122** (2000) 6520–6521; b) F. Márquez, V. Martí, E. Palomares, H. García, W. Adam, *J. Am. Chem. Soc.* **124** (2002) 7264–7265; c) F. Márquez, M.J. Sabater, *J. Phys. Chem. A* **109** (2005) 1559–1563.
- [14] See S.I. for the synthesis and characterization of MSN(TMS)-AP-Pt1.
- [15] H.E.B. Lempers, R.A. Sheldom, *J. Catal.* **109** (1988) 62–69.
- [16] a) L. Furst, B.S. Matsuura, J.M.R. Narayanam, J.W. Tucker, C.R.J. Stephenson, *Org. Lett.* **12** (2010) 3104–3107; b) R. Martínez-Haya, M.A. Miranda, M.L. Marin, *Eur. J. Org. Chem.* (2017) 2164–2169.
- [17] D.A. Nicewicz, D.W.C. MacMillan, *Science* **322** (2008) 77–80.
- [18] a) M. Neumann, S. Földner, B. König, K. Zeitler, *Angew. Chem., Int. Ed.* **50** (2011) 951–954; b) K. Fidal, C. Ceballos, A. Falguières, M. Sylla-Iyarreta Veitia, A. Guy, C. Ferroud, *Green Chem.* **14** (2012) 1293–1297;

- c) M. Cherevatskaya, M. Neumann, S. Földner, C. Harlander, S. Kümmel, S. Dankesreiter, A. Pfitzner, K. Zeitler, B. König, *Angew. Chem., Int. Ed.* 51 (2012) 4062–4066;
- d) P. Riente, M. Matas Adams, J. Albero, E. Palomares, M.A. Pericàs, *Angew. Chem., Int. Ed.* 53 (2014) 9613–9616;
- e) A. Gualandi, M. Marchini, L. Mengozzi, M. Natali, M. Lucarini, P. Ceroni, P.G. Cozzi, *ACS Catal.* 5 (2015) 5927–5931;
- f) T. Rigotti, A. Casado-Sánchez, S. Cabrera, R. Pérez-Ruiz, M. Liras, V.A. de la Peña O'Shea, J. Alemán, *ACS Catal.* 8 (2018) 5928–5940.
- [19] The obtained alkylated products **4a** and **4b** were almost racemic due to the acid character of the silica material, which provokes their enolization and therefore the loss of the enantiomeric excess.
- [20] Miura and Shishido have recently described that a higher reaction rate of polar substrates than apolar ones is attributed to the hydrophilic environment in the catalytic site of the silica mesoporous material H. Miura, S. Kameyama, D. Komori, T. Shishido, *J. Am. Chem. Soc.* 141 (2019) 1636–1645.